

# Graduate School Project Report

## Zel'dovich Approximation

Sujatha Ramakrishnan

Project Guide: Prof. Aseem Paranjape

July 21, 2017

# Contents

<b>1</b>	<b>Introduction</b>	<b>1</b>
<b>2</b>	<b>Theory</b>	<b>3</b>
2.1	Lagrangian Perturbation Theory . . . . .	3
2.2	Web Classification using Tidal Tensor . . . . .	5
<b>3</b>	<b>Techniques</b>	<b>6</b>
3.1	Numerical Realisation of the Zel'dovich Approximation . . . . .	6
3.1.1	Obtaining Displacement Field . . . . .	6
3.1.2	Obtaining Velocity Field . . . . .	7
3.1.3	Creating Gaussian Random Density Field . . . . .	7
3.1.4	Obtaining Tidal Tensor and WebClassification . . . . .	8
3.2	Interpolation Techniques . . . . .	8
3.2.1	Nearest Grid Point ( NGP) . . . . .	8
3.2.2	Smoothing of NGP . . . . .	8
3.2.3	Cloud in a Cell (CIC) . . . . .	9
<b>4</b>	<b>Numerical Results</b>	<b>10</b>
4.1	One Dimensional Zel'dovich Approximation . . . . .	10
4.1.1	Collisionless particles . . . . .	10
4.1.2	1D Collapse of a plain wave . . . . .	11
4.2	Two Dimensional Zel'dovich Approximation . . . . .	11
4.3	Three Dimensional Zel'dovich Approximation . . . . .	11
4.3.1	Power Spectrum . . . . .	11
4.3.2	Formation of structures . . . . .	14
4.3.3	Web Classification . . . . .	16
<b>5</b>	<b>Summary and Future Prospects</b>	<b>20</b>
<b>6</b>	<b>References</b>	<b>21</b>

## **Abstract**

In this project the Zel'dovich approximation has been studied in one, two and three dimensional spaces and its features such as formation of caustics , non linear collapse into nodes, filaments, sheets, and voids, web classification and the limitations imposed by the numerics are explored.

### **Acknowledgements**

I am extremely grateful to Prof.Aseem Paranjape for giving me a very interesting project to work on and for mentoring me throughout patiently for these few months. I would like to sincerely thank him for all the long hour discussions from which I have benefited greatly.

I would also like to thank Niladri Paul for his help with the project at various occasions . Special thanks to the members of IUCAA for providing a congenial environment.

# Chapter 1

## Introduction

It is believed that the universe was initially very homogenous with small density fluctuations which grew to form the structures that we observe today. Here we are interested in the anisotropies in the cosmic distribution of dark matter. Since dark matter does not interact with photons or baryons, they satisfy collisionless boltzmann equation. Thus dark matter unlike photons can always be described as a fluid. Moments of the boltzmann equation gives rise to the fluid equations. Linear perturbation theory involves perturbative treatment of these equations upto first order. Such a treatment gives rise to growing and decaying solutions in the  $\Lambda$ CDM model of cosmology. Given that all fluctuations were small at early times, it is resonable to assume that at more recent epochs only the growing mode has a significant amplitude. If  $\rho$  is the local density and  $\bar{\rho}$  is the average density then  $\delta(\mathbf{x}, t) = \rho/\bar{\rho} - 1$  is the density perturbations and its linear solution is given by,

$$\delta(\mathbf{x}, a) = D_1^+(a)\delta_i(\mathbf{x}) \quad (1.1)$$

where  $\delta_i(\mathbf{x})$  is the density perturbation at some initial time  $t_i$ , and  $D_1^+(a)$  (also known as the growth factor) is normalised such that  $D_1^+(a_i) = 1$ . The growth factor has the form,

$$D_1^+(a) = \frac{5}{2}\Omega_{m0}\frac{H}{H_0}\int_0^a \frac{da'}{[a'H(a')/H_0]^3} \quad (1.2)$$

Where  $H_0$  is the Hubble parameter today and  $\Omega_{m0}$  is the matter density parameter today. In  $\Lambda$ CDM model,  $D_1^+(a)$  can be written in terms of the hypergeometric function  ${}_2F_1$  as,

$$D_1^+(a) = \frac{a^{5/2}}{\sqrt{\Omega_{m0}}} \frac{H}{H_0} {}_2F_1\left(\frac{5}{6}, \frac{3}{2}, \frac{11}{6}, -a^3 \frac{\Omega_\Lambda}{\Omega_{m0}}\right) \quad (1.3)$$

where  $\Omega_\Lambda$  is the cosmological constant parameter. This solution works well as long as  $(\delta \ll 1)$ . If one wants to do better they must include higher order perturbations. Another limitation of linear theory is that it does not lead to non linear structures that

we observe in the universe today: the final density field is just a scaled up version of the initial density field. Zel'dovich Approximation (1970) is an alternate formulation of the linear perturbative equations which can give accurate description of higher non linear density perturbations. It predicts the rich structure of voids, clusters, sheets and filaments. Thus it is used to generate set of initial conditions around redshift of 100 for N-body simulations. It also provides qualitatively good match to N-body simulation results for later times (smaller redshifts) especially at large scales [1]. The report is structured as follows. Chapter 2 describes the mathematical formulation of Zel'dovich approximation (abbreviated as ZA). Chapter 3 discusses the techniques to implement it and Chapter 4 gives the numerical results and analysis. We conclude in Chapter 5. We will be using the flat  $\Lambda$ CDM model throughout the report.

# Chapter 2

## Theory

### 2.1 Lagrangian Perturbation Theory

Zel'dovich approximation provides a formulation of the linear perturbation theory which allows us to handle non linear density contrasts. This is achieved by moving from Eulerian to Lagrangian framework. In this framework the coordinates describe the initial position of the fluid elements and the dynamic equations give us the peculiar velocity and displacement of these fluid elements from their initial position. The mapping from Lagrangian coordinates ( $\mathbf{q}$ ) to Eulerian coordinates( $\mathbf{x}$ ) is given by:

$$\mathbf{x}(\mathbf{q}, t) = \mathbf{q} + \boldsymbol{\psi}(\mathbf{q}, t) \quad (2.1)$$

where  $\boldsymbol{\psi}(\mathbf{q}, t)$  is known as the displacement field. Let  $\bar{\rho}_m$  be the density of the fluid element initially at position  $\mathbf{q}$ . At this time the density fluctuations are so small that this  $\bar{\rho}_m$  can be taken to be equal to the average density of the entire fluid. Let  $\rho_m$  be the density of this fluid element when it has moved to position  $\mathbf{x}$ . Mass conservation at the two positions (two coordinates) implies that

$$\rho_m d^3x = \bar{\rho}_m d^3q \quad (2.2)$$

$$(1 + \delta)d^3x = d^3q \quad (2.3)$$

Here,  $d^3x$  is the infinitesimal Eulerian volume occupied at position  $x$  by the fluid element that started from  $q$  with infinitesimal Lagrangian volume  $d^3q$ . From eqn[2.3] we can see that the jacobian of coordinate transformation is ,

$$J \equiv \text{Det} \left( \frac{\partial \mathbf{x}_i}{\partial \mathbf{q}_j} \right) \quad (2.4)$$

$$= \text{Det} (\delta_{ij} + \psi_{i,j}) \quad (2.5)$$

$$= \frac{1}{1 + \delta} \quad (2.6)$$

The equation of motion of a fluid element in Eulerian coordinates and conformal time is given by,

$$\frac{d^2\mathbf{x}}{d\tau^2} + \mathcal{H}\frac{d\mathbf{x}}{d\tau} = -\nabla\Phi \quad (2.7)$$

$$(2.8)$$

Recasting this into Lagrangian coordinates and taking divergence gives,

$$J(\delta_{ij} + \psi_{i,j})^{-1} \nabla_{\mathbf{q}_j} \left( \frac{d^2\psi_i}{d\tau^2} + \mathcal{H}\frac{d\psi_i}{d\tau} \right) = \frac{3}{2}\Omega_m\mathcal{H}^2(J-1) \quad (2.9)$$

To obtain the linear solution we can expand the displacement field perturbatively and substitute in the equation above keeping track of first order terms,

$$\psi_i = \psi_i^{(1)} + \psi_i^{(2)} + \dots \quad (2.10)$$

On the left hand side we can set  $J = 1$  and  $(\delta_{ij} + \psi_{i,j})^{-1} \approx \delta_{ij}$  since it multiplies with terms which are atleast first order themselves. On the right hand side we can expand eqn[2.6] into a series and use the approximation.

$$J - 1 \approx -\delta^{(1)}(\mathbf{q}, \tau) \quad (2.11)$$

Making use of the identity  $\text{Det}(A) = e^{\text{Trace}(\ln A)}$ , the jacobian can also be written in another approximate form as follows.

$$\ln(\delta_{ij} + \psi_{i,j}) \approx \psi_{i,j} + \mathcal{O}(\psi_{i,j})^2 \quad (2.12)$$

$$\text{Trace}(\ln(\delta_{ij} + \psi_{i,j})) \approx \text{Trace}(\psi_{i,j}) \quad (2.13)$$

$$\approx \psi_{i,i} \quad (2.14)$$

$$\approx \nabla_{\mathbf{q}} \cdot \psi \quad (2.15)$$

$$J = \text{Det}(\delta_{ij} + \psi_{i,j}) \quad (2.16)$$

$$= \exp(\text{Trace}(\ln(\delta_{ij} + \psi_{i,j}))) \quad (2.17)$$

$$= \exp(\text{Trace}(\psi_{i,j})) \quad (2.18)$$

$$= 1 + \nabla_{\mathbf{q}} \cdot \psi^{(1)} \quad (2.19)$$

Comparing eqn[2.11] and eqn[2.19], we get

$$\delta^{(1)}(\mathbf{q}, \tau) = -\nabla_{\mathbf{q}} \cdot \psi^{(1)}(\mathbf{q}, \tau) = D_1^+(\tau)\delta^{(1)}(\mathbf{q}). \quad (2.20)$$

Here  $D_1^+(\tau)$  is normalised to be unity at some time  $\tau_0$  when the perturbation was equal to  $\delta(\mathbf{q})$ . The linearised equation is,

$$\frac{d^2\nabla_{\mathbf{q}}\psi}{d\tau^2} + \mathcal{H}\frac{d\nabla_{\mathbf{q}}\psi}{d\tau} = -\frac{3}{2}\Omega_m\mathcal{H}^2\delta^{(1)}(\mathbf{q}, \tau) \quad (2.21)$$

$$= \frac{3}{2}\Omega_m\mathcal{H}^2\nabla_{\mathbf{q}} \cdot \psi(\mathbf{q}, \tau) \quad (2.22)$$

The growing solution to this equation is already known from the linear perturbation theory to be,

$$\nabla_{\mathbf{q}} \psi^{(1)}(\mathbf{q}, \tau) = D_1^+(\tau) \nabla_{\mathbf{q}} \psi^{(1)}(\mathbf{q}) \quad (2.23)$$

where  $\psi^{(1)}(\mathbf{q})$  is the value of  $\psi$  at the time  $\tau_0$  mentioned earlier. Since linear theory cannot sustain a rotational component of velocity which is the time derivative of displacement vector, we will assume an irrotational displacement vector,i.e,

$$\psi^{(1)}(\mathbf{q}) = \nabla_{\mathbf{q}} \psi^{(1)}(\mathbf{q}) \quad (2.24)$$

Comparing eqn [2.20] to eqn [2.23] and replacing the vector displacement field with the scalar displacement field from eqn[2.24], we get

$$\nabla_{\mathbf{q}}^2 \psi^{(1)}(\mathbf{q}) = -\delta^{(1)}(\mathbf{q}) \quad (2.25)$$

By solving this equation we can get the scalar  $\psi$  and the final position and velocity of the fluid element is now given by,

$$\mathbf{x}(\mathbf{q}, t) = \mathbf{q} + \nabla \psi(\mathbf{q}, t) \quad (2.26)$$

$$\mathbf{u} = \frac{dD_1^+}{d\tau} \nabla_{\mathbf{q}} \psi^{(1)} \quad (2.27)$$

## 2.2 Web Classification using Tidal Tensor

We can learn more about the kind of deformation the fluid element undergoes by studying the Jacobian more carefully. From the definitions of the jacobian in equations [2.5] and [2.6] we get,

$$1 + \delta(\mathbf{q}, \tau) = \frac{1}{\text{Det}(\delta_{ij} + \psi_{i,j})} \quad (2.28)$$

$$\psi_{i,j}(\mathbf{q}, \tau) \approx \psi_{i,j}^{(1)}(\mathbf{q}, \tau) = D_1^+(\tau) \partial_{ij} \psi^{(1)}(\mathbf{q}) \quad (2.29)$$

Here  $\partial_{ij} \psi^{(1)}(\mathbf{q})$  is defined as the tidal tensor. Let  $\lambda_1, \lambda_2, \lambda_3$  be the eigen values of the tidal tensor. Since the determinant of the jacobian is the product of its eigen values eqn [2.28] becomes

$$1 + \delta(\mathbf{q}, \tau) = \frac{1}{\prod_{i=1}^3 (1 + D_1^+(\tau) \lambda_i(\mathbf{q}))} \quad (2.30)$$

From this expression we can see that depending on the relative magnitude of these eigenvalues, the Zel'dovich approximation leads to planar collapse (one negative eigenvalue ), filamentary collapse (two negative eigenvalues), or complete collapse (all eigenvalues negative). If all eigenvalues are positive, then the evolution corresponds to an underdense region, eventually reaching  $\delta = -1$ .

# Chapter 3

## Techniques

### 3.1 Numerical Realisation of the Zel'dovich Approximation

In cosmological simulations, dark matter is usually represented as discrete fluid element of equal masses initially placed at the vertex points of a Cartesian uniform lattice to start with. Given an initial density field it is possible to find the displacement of each of these particles from its lattice point so as to mimic this density perturbation field using the Zel'dovich approximation.

#### 3.1.1 Obtaining Displacement Field

Recall that the eqn [2.25] in Fourier space would look like,

$$k^2 \tilde{\psi}^{(1)}(\mathbf{k}) = \tilde{\delta}^{(1)}(\mathbf{k}) \quad (3.1)$$

$$\psi^{(1)}(\mathbf{q}) = \int \frac{e^{i\mathbf{k}\cdot\mathbf{q}}}{(2\pi)^3} \frac{\tilde{\delta}^{(1)}(\mathbf{k})}{k^2} d^3k \quad (3.2)$$

$$\nabla_{\mathbf{q}} \psi^{(1)}(\mathbf{q}) = \int \frac{e^{i\mathbf{k}\cdot\mathbf{q}}}{(2\pi)^3} i\mathbf{k} \frac{\tilde{\delta}^{(1)}(\mathbf{k})}{k^2} d^3k \quad (3.3)$$

Thus we can get the displacement field by systematically taking numerical inverse Fourier transform of the given density field, multiplying it by  $i\mathbf{k}/k^2$  and converting this quantity back to real space by applying numerical Fourier transform. In this project the fast Fourier transform algorithm is used from the numpy library of Python.

### 3.1.2 Obtaining Velocity Field

The velocity can be obtained from eqn[2.26],

$$\mathbf{v} = \frac{d\mathbf{x}}{d\tau} \quad (3.4)$$

$$= \frac{dD_1^+(\tau)}{d\tau} \nabla_{\mathbf{q}} \psi^{(1)}(\mathbf{q}) \quad (3.5)$$

$$= \nabla_{\mathbf{q}} \psi^{(1)}(\mathbf{q}) \frac{H_0^2}{H} \left[ \frac{5}{2} \frac{\Omega_{m0}}{a} - \frac{3}{2} \Omega_{m0} a^{-2} D_1^+(\tau) \right] \quad (3.6)$$

The final equation can be obtained by differentiating the growth factor whose form was shown in eqn[1.3].

### 3.1.3 Creating Gaussian Random Density Field

In standard cosmological models, the initial perturbation density field is Gaussian distributed. In real space the probability distribution of the density fluctuations is a multidimensional Gaussian. There is correlation between the nearby density fluctuations. But in Fourier space each  $k$  mode equation is uncoupled with other  $k$  modes in the linear perturbation theory equations. Hence the Fourier counterpart density fluctuations are independent. The correlation of Fourier space density fluctuations is related to the power spectrum by

$$\langle \delta(\mathbf{k}) \delta(\mathbf{k}') \rangle = (2\pi)^3 \delta_D(\mathbf{k} - \mathbf{k}') P(\mathbf{k}) \quad (3.7)$$

While going from continuous to discrete case the continuous  $\delta(\mathbf{k})$  can be discretised and replaced with  $\delta_{\mathbf{k}} \frac{(2\pi)^3}{(\Delta k)^3}$ .  $\delta_{\mathbf{k}}$  is the Discrete Fourier Transform of  $\delta(x)$ .  $\Delta k$  is the smallest  $k$  mode probed and is equal to  $(2\pi)^3/L^3$  and  $L$  is the length of the real space interval. We can relate the power spectrum to the variance of the discrete  $\delta_{\mathbf{k}}$  as follows.

$$\langle \delta_{\mathbf{k}}^2 \rangle = \frac{dk^3}{(2\pi)^3} P(\mathbf{k}) \quad (3.8)$$

Also the mean of  $\delta_{\mathbf{k}}$  is given by

$$\langle \delta_{\mathbf{k}} \rangle = \langle \text{DFT}(\delta_{\mathbf{x}}) \rangle = \text{DFT} \langle \delta_{\mathbf{x}} \rangle = 0 \quad (3.9)$$

Thus we can create Gaussian random variable  $\delta_{\mathbf{k}}$  of mean 0 and variance related to power spectrum, take inverse Fourier transform of it to get the Gaussian real space density field. Care should be taken to incorporate properties into  $\delta_{\mathbf{k}}$  that make its Fourier transform real.

### 3.1.4 Obtaining Tidal Tensor and WebClassification

We already know from eqn[3.3]

$$\psi_{,i}^{(1)}(\mathbf{q}) = \int \frac{e^{i\mathbf{k}\cdot\mathbf{q}}}{(2\pi)^3} i\mathbf{k}_i \frac{\tilde{\delta}^{(1)}(\mathbf{k})}{k^2} d^3k \quad (3.10)$$

$$\psi_{,ij}^{(1)}(\mathbf{q}) = \int \frac{e^{i\mathbf{k}\cdot\mathbf{q}}}{(2\pi)^3} (-\mathbf{k}_i \mathbf{k}_j) \frac{\tilde{\delta}^{(1)}(\mathbf{k})}{k^2} d^3k \quad (3.11)$$

Thus the tidal tensor can be obtained by taking inverse discrete Fourier transform of  $-\mathbf{k}_i \mathbf{k}_j \frac{\tilde{\delta}^{(1)}(\mathbf{k})}{k^2}$ . Web Classification is the identification of the fluid element as a void, filament, sheet or node by its number of positive/negative eigen values. Implementing this is fairly straightforward with numpy.linalg package of Python.

## 3.2 Interpolation Techniques

Once particles are displaced from the lattice points, the fluid is not homogenous anymore. There are density fluctuations imprinted in them. The various interpolation methods are useful to assign densities to the grid cells. Let the 1 D particle shape  $S(x)$  be the mass density at a distance  $x$  from the particle for cell size  $\Delta x$ . Three types of interpolation schemes are discussed here.

### 3.2.1 Nearest Grid Point ( NGP )

Particles are point like and all the particle's mass is assigned to the single grid cell that contains it:

$$S(x) = \frac{1}{\Delta x} \delta\left(\frac{x}{\Delta x}\right)$$

It is seen that if the separation between particles are held constant and the particles are displaced with respect to the mesh grid, then the interpolation value fluctuates with a period given by the cell width  $\Delta x$ . It is this loss of displacement invariance which affects the physical reality of this interpolation [4].

### 3.2.2 Smoothing of NGP

The errors in NGP arises from the crudeness of density assignment and smoothing can help in identifying large scale structures which would otherwise be hidden in high-amplitude small-scale noise. Any density function  $\rho$  can be averaged over a length scale  $R$  by convolving it with a normalised window function as shown below:

$$\rho_R(x_0) = \int w_R(x - x_0) \rho(x) dx$$

### 3.2.3 Cloud in a Cell (CIC)

Particles are extended and of one grid cell size dimension.

$$\begin{aligned} S(x) &= \frac{1}{\Delta x}, & |x| < \frac{1}{2}\Delta x \\ &= 0, & \text{otherwise} \end{aligned}$$

CIC is much more smoother than NGP, the amplitude fluctuations in interpolated values is much more reduced as compared to NGP as the particles are displaced with respect to the mesh grid.

# Chapter 4

## Numerical Results

### 4.1 One Dimensional Zel'dovich Approximation

One dimensional Zel'dovich approximation would be equivalent to a three dimensional scenario, where the density fluctuations in the other two directions are zero. Thus 1D ZA would result in collapse of parallel sheets of matter in 3D. It is interesting to study as its full phase space trajectory can be visualised. Before looking at the trajectory of gravitating particles using ZA, it would be useful to study the trajectory of collisionless non interacting particles.

#### 4.1.1 Collisionless particles

Fig[4.1] shows different time shots of the phase space trajectory initially chosen to be sinusoidal and let to evolve. If  $f(x, p)$  denotes the phase space distribution at  $x_0$  and  $p_0$ ,

$$f(x, p) = \delta(x - x_0)\delta(p - \sin(x_0)) \quad (4.1)$$

$$\langle p \rangle_{x=x_0} = \int p f(x, p) dx dp \quad (4.2)$$

$$= \int p \delta(x - x_0)\delta(p - \sin(x_0)) dx dp \quad (4.3)$$

$$= \sin(x_0) \quad (4.4)$$

Thus in a region  $dx$  around each point  $x_0$  the average velocity is equal to the single velocity of all the particles at that point :  $\sin(x_0)$ . Since the particles do not interact their velocities will remain the same with time. Only the position changes with time either towards left or right depending on the sign of velocity. After a certain time shown in the extreme right of Fig[4.1] the particles in some regions of  $x$  start crossing each other. Such regions in  $x$  space are called multi-streaming regions. The boundaries of the multi-streaming regions where the phase sheet becomes vertical are termed 'caustics'. The density here is infinite. The average velocity now inside the multistreaming region will be sum average of two distinct positive and negative velocity will not correspond to velocity of any particle in this region.

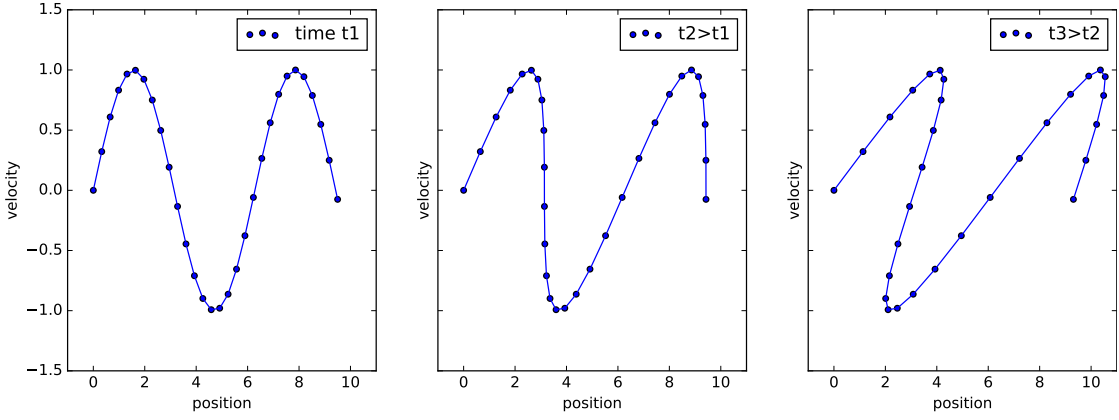


Figure 4.1: Particles initially having a sinusoidal phase space trajectory are let to evolve without collision or gravity interaction. Multistreaming regions can be seen to form in the extreme right panel

#### 4.1.2 1D Collapse of a plain wave

Particles initialised as a plane wave in phase space are let to evolve using ZA. A reason why zeldovich approximation works so well in 3d is because it is the exact solution in one dimension. In Fig[4.2], in addition to formation of caustics the increase in velocity is also seen with increasing time.

## 4.2 Two Dimensional Zel'dovich Approximation

The 2D ZA is shown in Figure above, a toy power spectrum of the form  $k \exp(-k/k_c)$  is used since we can expect prominent structures in the length scale characterised by  $k_c$ . We can see growing filamentary structures and shell crossing.

## 4.3 Three Dimensional Zel'dovich Approximation

### 4.3.1 Power Spectrum

The fitting form of Transfer Function Bardeen, Bond, Kaiser, and Szalay(1986,BBKS) is used [2]:

$$T(q \equiv k/\Gamma h Mpc^{-1}) = \frac{\ln[1 + 2.34q]}{(2.34q)} \left[ 1 + 3.89q + (16.2q)^2 + (5.47)^3 + (6.71)^4 \right]^{-0.25} \quad (4.5)$$

The power spectrum of density fluctuations at any redshift is given by:

$$P(k, z) = Ak^{ns} T^2(k) \left( \frac{D_1^+(z)}{D_1^+(z=0)} \right)^2 \quad (4.6)$$

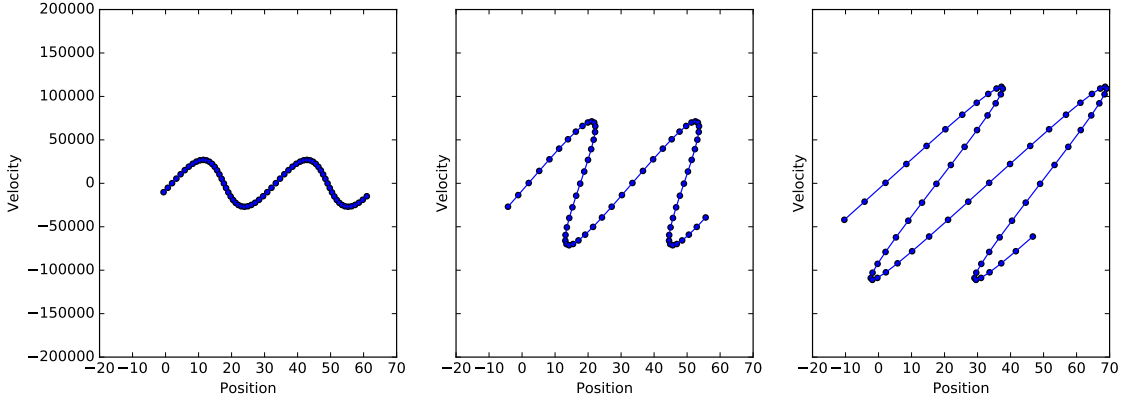


Figure 4.2: Particles initially having a sinusoidal phase space trajectory are let to evolve using Zel'dovich approximation. Though the initial perturbation is unrealistic 1 d analysis allows us to visualize the phase space evolution and formation of caustics in the presence of gravity

The power  $ns = 0.96$  comes from the primordial power spectrum. Fig[4.4] left panel shows the form of the power spectrum at redshift 0. The smaller modes which entered the horizon later than the matter- radiation equality have retained their primordial power. The larger modes that entered the horizon much before the matter radiation equality and their power got damped as the radiation pressure wipes out coherence.

### Structures form earlier at small scales than large scales

The autocorrelation function is defined as

$$\xi(\mathbf{x}_1, \mathbf{x}_2) = \langle \delta(\mathbf{x}_1) \delta(\mathbf{x}_2) \rangle \quad (4.7)$$

Due to homogeneity and isotropy the auto correlation function depends only on the separation between the point  $\mathbf{x}_1$  and  $\mathbf{x}_2$ .

$$\xi \equiv \xi(x) \quad (4.8)$$

where  $x = |\mathbf{x}_1 - \mathbf{x}_2|$

$$\xi(0) = \langle \delta(\mathbf{x}) \delta(\mathbf{x}) \rangle \quad (4.9)$$

would give the variance in the density fluctuation. The Power Spectrum is defined as the Fourier transform of correlation function. Hence the variance of density fluctuation

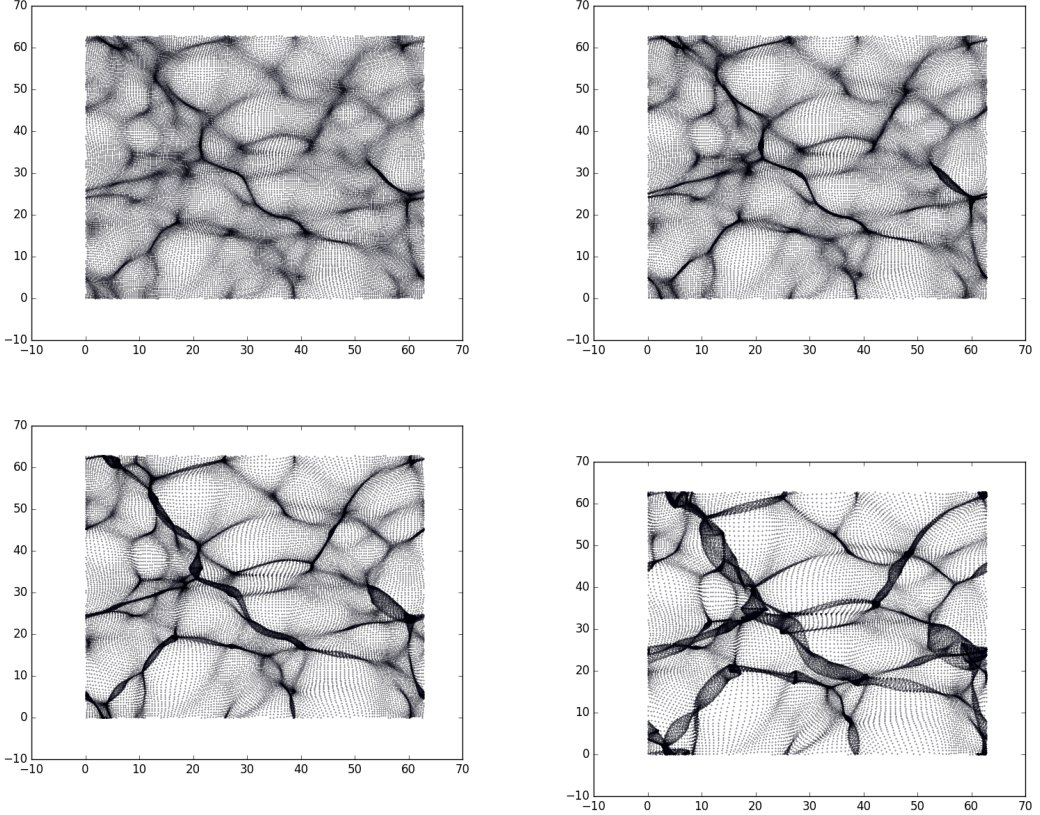


Figure 4.3: Figures denote the time evolution of particles in the order top left ,top right , bottom left, bottom right. A total of  $64^3$  particles are taken.

would just be the Power Spectrum integrated in Fourier space,i.e,

$$\langle \delta(x)\delta(x) \rangle = \int \frac{P(k)}{(2\pi)^3} d^3k \quad (4.10)$$

$$= \int \frac{P(k)}{(2\pi)^3} 4\pi k^2 dk \quad (4.11)$$

$$= \int \frac{P(k)}{(2\pi)^3} 4\pi k^3 \frac{dk}{k} \quad (4.12)$$

$$= \int \frac{P(k)}{2\pi^2} k^3 d \ln k \quad (4.13)$$

The quantity  $\Delta^2 \equiv \frac{P(k)}{2\pi^2} k^3$  is dimensionless which makes it useful to handle rather than the power spectrum. The area under the curve  $\Delta^2$  vs  $\log k$  at an interval centered around a particular  $k$  will give the strength of the density fluctuation at that particular length scale. Thus simply comparing the magnitude or power of  $\Delta^2$  at different  $k$  values

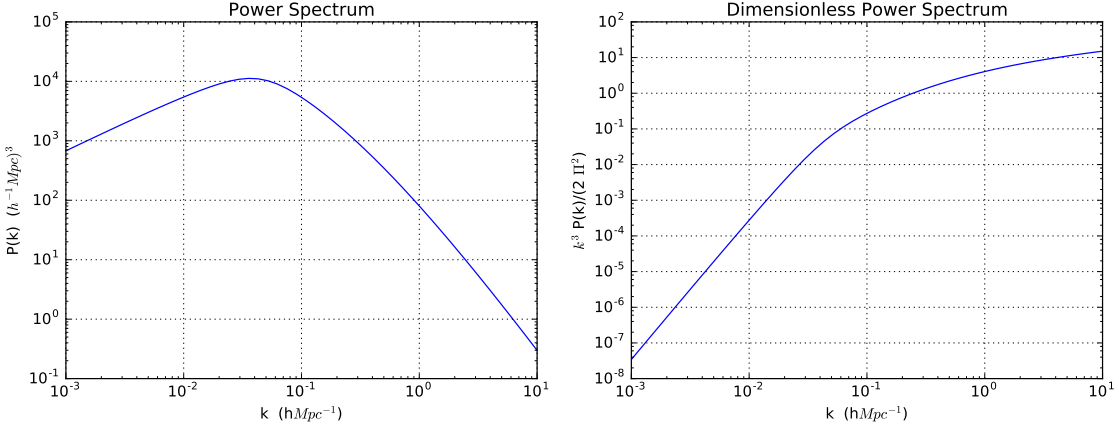


Figure 4.4: Power Spectrum obtained using the BBKS Transfer function

tells us which length scales have higher density fluctuation. In Fig[4.4] there is more power in  $\Delta^2$  for smaller and smaller scales (higher  $k$  values). Hence small length scale density fluctuations form structures earlier than large scales. This is demonstrated in the numerical realisation of Zel'dovich approximation in the next section.

### 4.3.2 Formation of structures

In Fig[4.5] scatter plots of 3D ZA is done to equal number of particles ( $N=40$ ) but at different length scales. We can observe the manifestation of the effect described in previous section. Since we can only do ZA in finite box size, we can only probe the power from  $k$  modes starting from the largest length scale of the box ( $k_{min} = 2\pi/L_{box}$ ) to the smallest length scale of the box ( $k_{max} = 2\pi/dx$ ). This places constrain on the interval which is probed in the  $\log \Delta^2$  vs  $\log k$  plot.

$$\log k_{max} - \log k_{min} = \log \left( \frac{k_{max}}{k_{min}} \right) \quad (4.14)$$

$$= \log \frac{L_{box}}{dx} \quad (4.15)$$

$$= \log N \quad (4.16)$$

Though the interval is constant the region it probes is determined by the box size. Hence smaller boxes such as the left panel of Fig[4.5] form structures earlier (At redshift =15) since they probe higher  $k$  modes which have larger power, whereas the largest box on the extreme right is highly uniform at this redshift and begins to show structures only around redshift 0.5. Also from these figures the shell crossing and dispersion can be seen to happen much early for smaller boxes compared to the large ones.

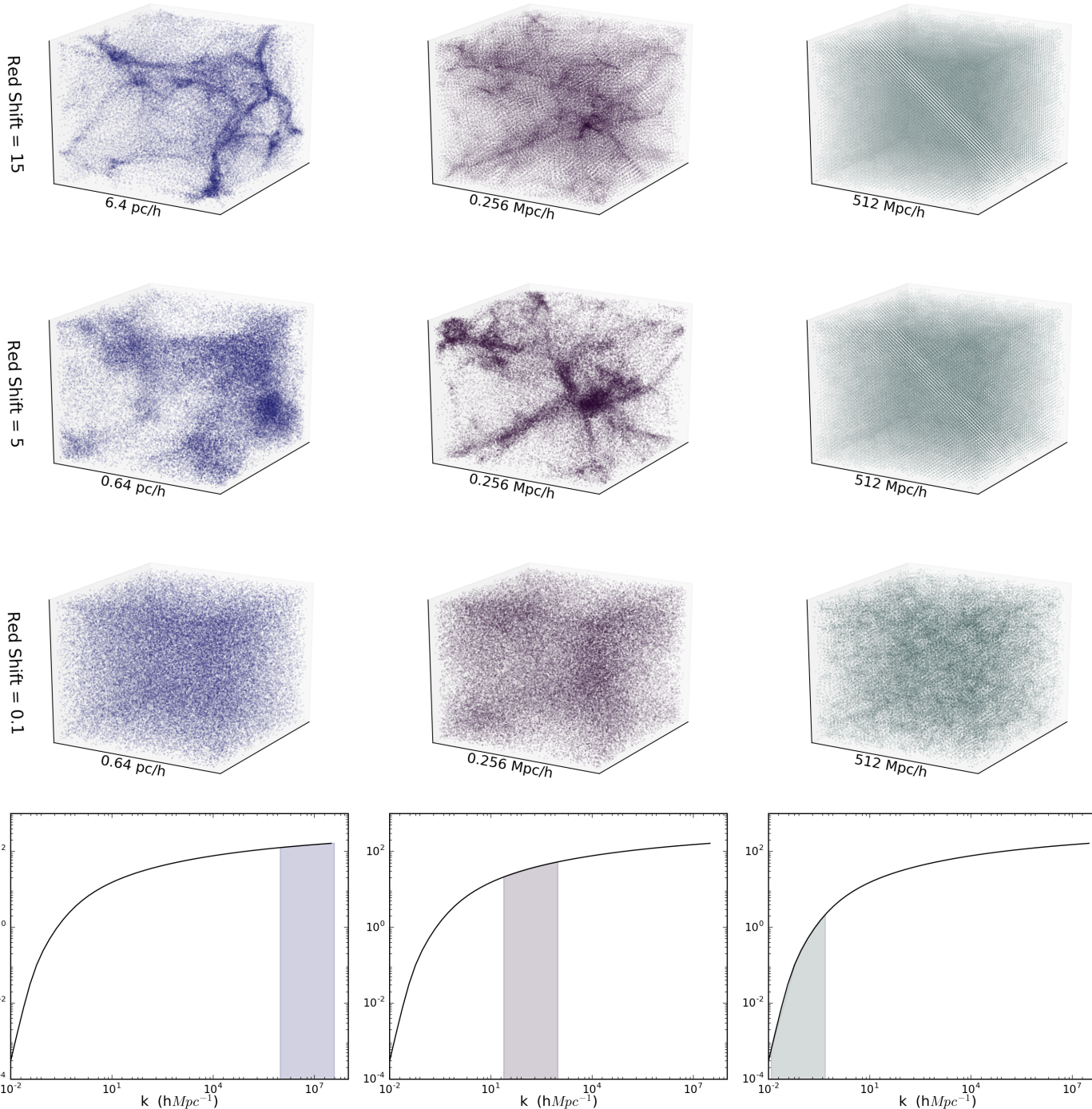


Figure 4.5: Particles displaced from cartesian lattice according to Zel'dovich approximation. Total number of particles =  $40 \times 40 \times 40$

Once the particles are displaced the density field is obtained using various techniques described in Chapter 2. Fig[4.6] shows one such interpolation for a box of size 1.28Mpc/h.

### 4.3.3 Web Classification

Each grid/particle in the initial density field is associated with a tidal tensor whose number of positive/negative eigen values can be used to classify the grid/particle as a void, filament, sheet or node. The same exercise can be repeated for the final density field obtained from the CIC interpolation scheme to classify the final grids as void, filament, sheet or node. Then the fraction of particles which were initially in node/sheet/filament/void classified grids and moved to other regions with other classification is calculated as shown in Fig[4.8]. In the initial condition, the fraction of voids and fraction of nodes are seen to be equal, so are the fraction of sheets and filaments. This results from the symmetry in the probability distribution of eigen values first given by Doroshkevich in 1970[5]. The probability measure  $p(\lambda_1, \lambda_2, \lambda_3)$  for the eigen values  $\lambda_1, \lambda_2, \lambda_3$  in any order, is

$$p(\lambda_1, \lambda_2, \lambda_3) = \frac{15^3}{8\pi\sqrt{5}\sigma^6} \exp\left(-\frac{3I_1^2}{\sigma^2} + \frac{15I_2}{2\sigma^2}\right) |\lambda_1 - \lambda_2| \times |\lambda_2 - \lambda_3| \times |\lambda_1 - \lambda_3| \quad (4.17)$$

where  $\sigma$  denotes the rms fluctuation of the smoothed field.,  $I_1 \equiv \lambda_1 + \lambda_2 + \lambda_3$ , and  $I_2 \equiv \lambda_1\lambda_2 + \lambda_2\lambda_3 + \lambda_1\lambda_3$ . From the above eqn[4.17], we can see equality of the following measures,

$$p(\lambda_1, \lambda_2, \lambda_3) = p(-\lambda_1, -\lambda_2, -\lambda_3) \quad (4.18)$$

$$p(\lambda_1, -\lambda_2, -\lambda_3) = p(-\lambda_1, \lambda_2, \lambda_3) \quad (4.19)$$

Eqn[4.18] explains why  $V_i$ -initial fraction of particles in void is equal to  $N_i$ -initial fraction of particles in node. Similarly Eqn[4.19] explains why  $F_i$ -initial fraction of particles in filaments is equal to  $N_i$ -initial fraction of particles in sheets. The final fractions of web classification does not follow the initial fractions. Although a conclusive reason for this is not understood we speculate that this could be due to the limitation in the interpolation technique used to obtain density for final web classification. In Fig[4.7] we can see a correlation between the intial density field and its webclassification in the top panel and a similar correspondence between final particle positions and the final webclassification. Also the similarity of final web classification (middle left panel) and the final particle positions are color coded with its initial web classification (bottom left panel) suggests that each particle carries along its initial classification to its final position.

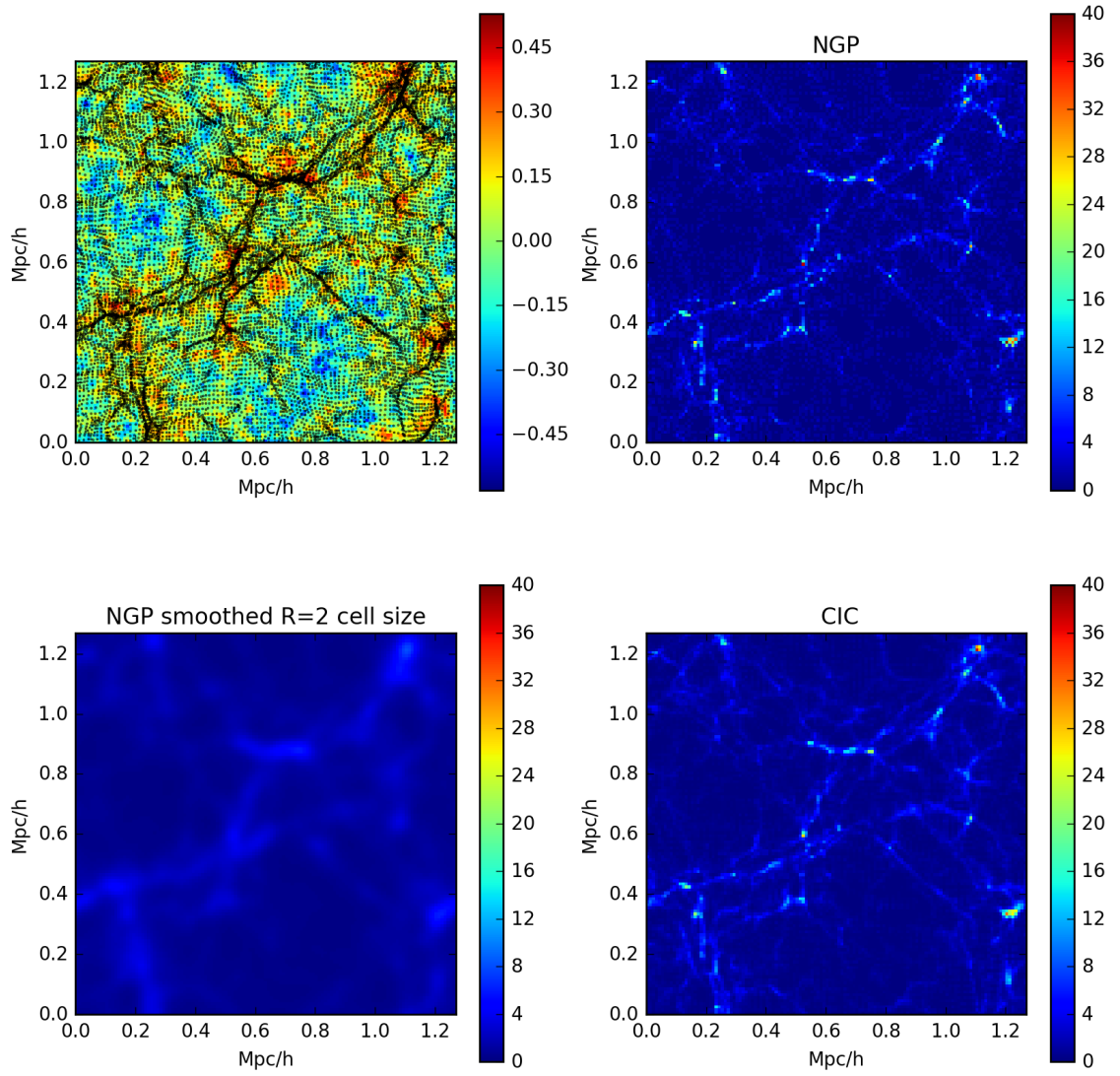


Figure 4.6: Interpolation after evolving a box of size 1.28 Mpc/h upto redshift 10. The top left panel shows the initial density field overplotted with particle positions at redshift 10. Notice how the particle positions lie on top of initially overdense(red) regions. Top right panel shows the NGP interpolation scheme. Bottom left and right are the smoothed NGP and CIC schemes respectively

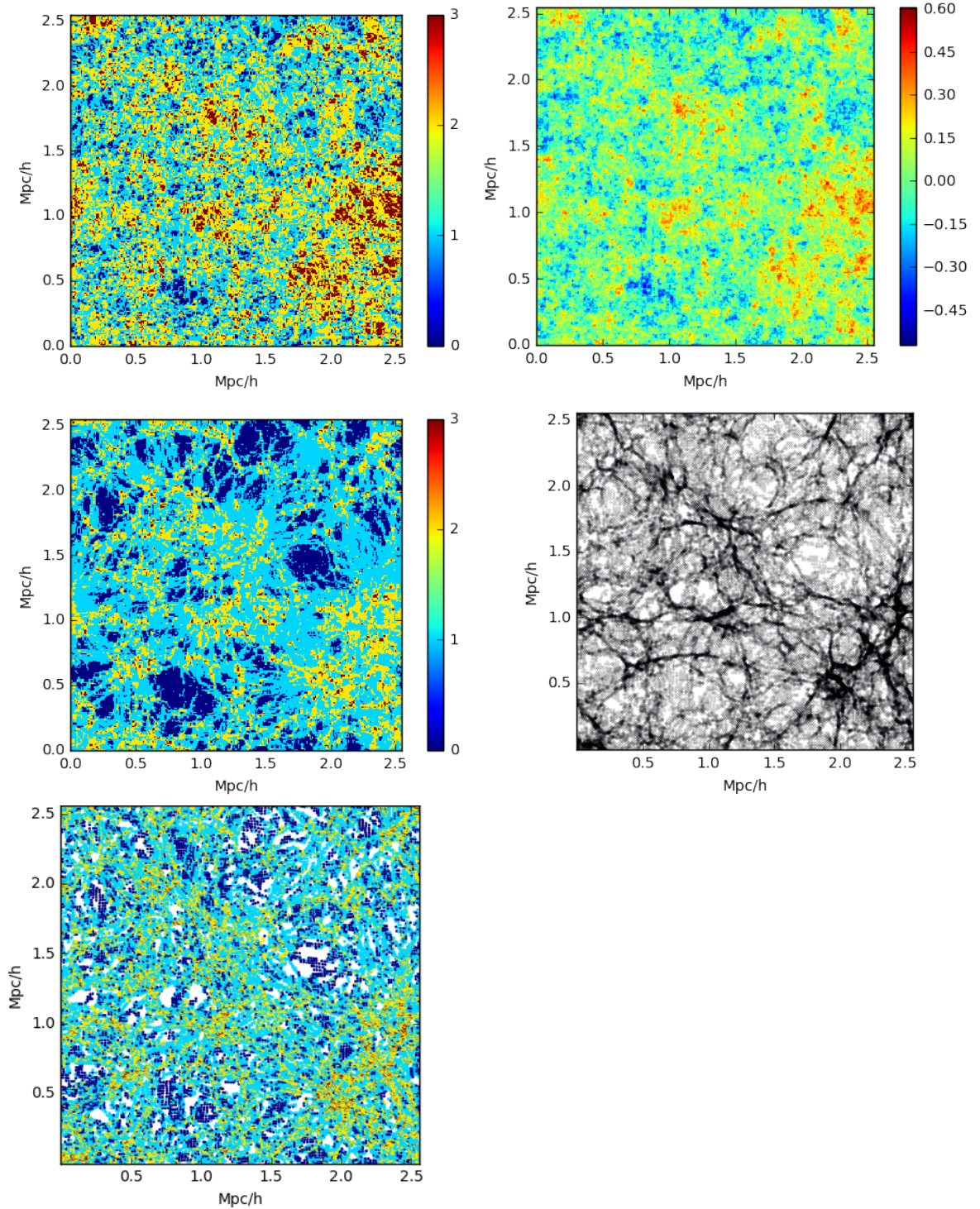


Figure 4.7: Top and middle left panel shows webclassification of initial and final cic density respectively. Colors denote the number of negative eigen values of the tidal tensor in that region. The top right panel shows the initial density field and the middle right panel shows particle positions. The bottom left plot is the final particles color coded with initial web classification. All plots are of unit cell thickness.

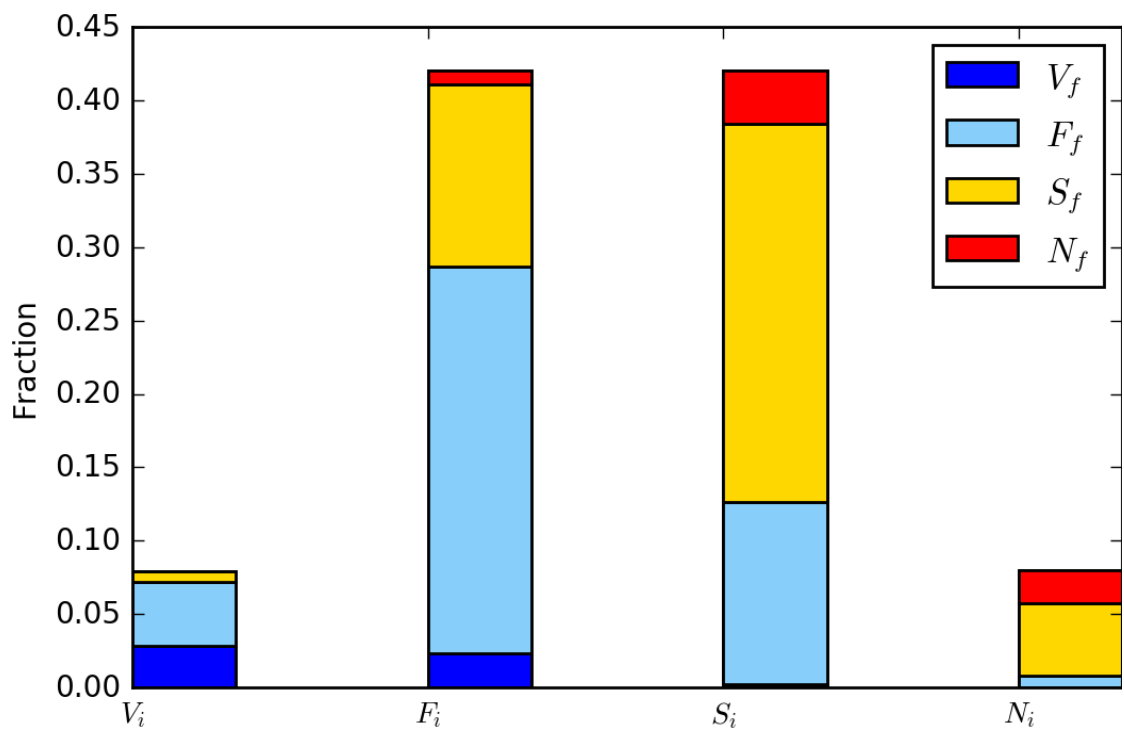


Figure 4.8: Figure gives the fraction of particles classified as voids,filaments,sheets and nodes in the initial density field and the final cic interpolated density field

## Chapter 5

# Summary and Future Prospects

The first order Lagrangian perturbation theory was studied in order to obtain the Zel'dovich approximation for displacing dark matter particles from their initial homogeneous distribution with small fluctuations. These small fluctuations appear as Gaussian density field with a power spectrum which is obtained using BBKS transfer function in this report. The final position of the displaced particles after ZA are used to obtain the final density field using various interpolation schemes. A faster way to implement the CIC scheme in Python is found. Over this course, properties of the ZA such as formation of caustics, strength of structures at different length scales and web classification were also studied .

In future, the second order perturbation theory is to be studied and is expected to provide remarkable improvement over the ZA as compared to full N-body simulations.

# Chapter 6

## References

1. Coles P., Melott A.L., Shandarin S.F., 1993, MNRAS, 260, 765
2. Modern Cosmology by Scott Dodelson
3. Galaxy Formation and Evolution by Houjun Mo, Frank van den Bosch, Simon White
4. Computer Simulation Using Particles by RW Hockney and JW Eastwood
5. Doroshkevich A.G., 1970, Astrofizika, 3 ,175
6. F. Bernardeau, S. Colombi, E. Gaztanaga, and R. Scoccimarro, Large scale structure of the universe and cosmological perturbation theory, Phys. Rep. 367, 1 (2002).
7. Zel'dovich, Y. 1970, A &A, 5, 84